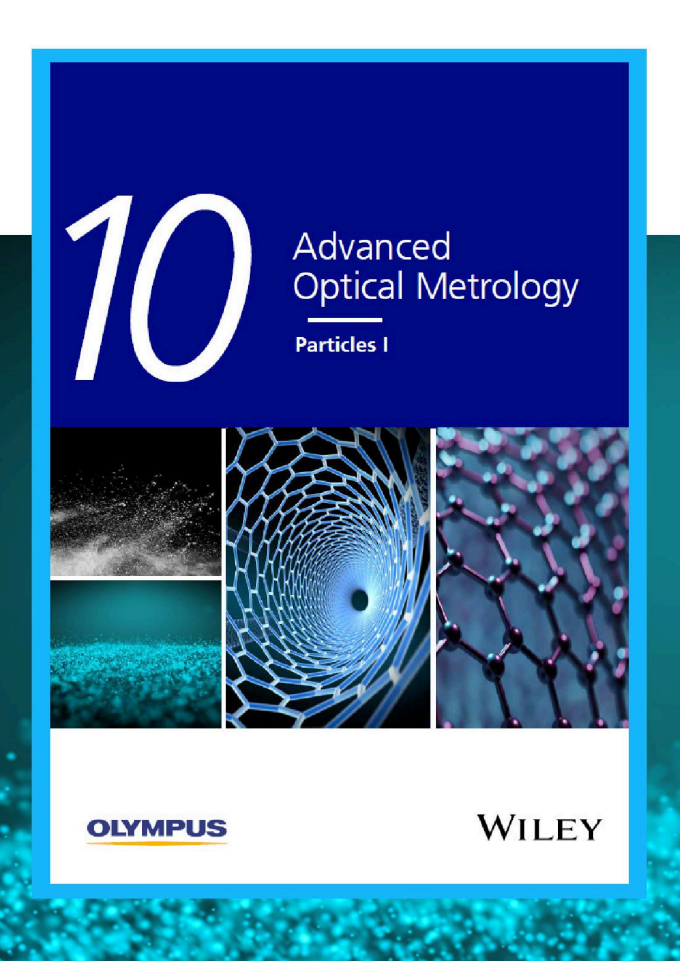
Particles Access the latest eBook



Particles: Unique Properties, Uncountable Applications

Read the latest eBook and better your knowledge with highlights from the recent studies on the design and characterization of microand nanoparticles for different application areas.

Access Now

OLYMPUS°

WILEY



Additives for Ambient 3D Printing with Visible Light

Dowon Ahn, Lynn M. Stevens, Kevin Zhou, and Zachariah A. Page*

With 3D printing, the desire is to be "limited only by imagination," and although remarkable advancements have been made in recent years, the scope of printable materials remains narrow compared to other forms of manufacturing. Light-driven polymerization methods for 3D printing are particularly attractive due to unparalleled speed and resolution, yet the reliance on high-energy UV/violet light in contemporary processes limits the number of compatible materials due to pervasive absorption, scattering, and degradation at these short wavelengths. Such issues can be addressed with visible-light photopolymerizations. However, these lower-energy methods often suffer from slow reaction times and sensitivity to oxygen, precluding their utility in 3D printing processes that require rapid hardening (curing) to maximize build speed and resolution. Herein, multifunctional thiols are identified as simple additives to enable rapid high-resolution visible-light 3D printing under ambient (atmospheric O2) conditions that rival modern UV/ violet-based technology. The present process is universal, providing access to commercially relevant acrylic resins with a range of disparate mechanical responses from strong and stiff to soft and extensible. Pushing forward, the insight presented within this study will inform the development of nextgeneration 3D-printing materials, such as multicomponent hydrogels and composites.

1. Introduction

Additive manufacturing is a rapidly expanding field that enables the production of complex 3D objects with unmatched speed and precision. Unlike traditional "subtractive" manufacturing processes, which require excessive time, energy, material, and equipment (for milling, carving, and machining), 3D printing operates in a simple "additive" fashion to create objects via successive growth.^[1–3] However, progress from prototyping to industrial manufacturing necessitates continued research efforts in the fundamental science and engineering of 3D printing to simultaneously decrease production time,^[4,5] broaden material scope,^[6,7] demonstrate energy efficient scalability,^[8] and enhance resolution,^[9,10] all with facile user-friendly operation.

Numerous additive methods that bring materials together with spatial control have been demonstrated, from deposition

D. Ahn, L. M. Stevens, K. Zhou, Z. A. Page Department of Chemistry The University of Texas at Austin 105 East 24th Street, Stop A5300, Austin, TX 78712, USA E-mail: zpage@utexas.edu

The ORCID identification number(s) for the author(s) of this article can be found under https://doi.org/10.1002/adma.202104906.

DOI: 10.1002/adma.202104906

and heating to light exposure. The utility of light is particularly attractive given the ability to create micrometer-sized features at low cost using inexpensive existing projection-based Digital Light Processing (DLP) and light-emitting diode liquid crystal display (LED/LCD) technologies. Both DLP and LED/LCD methods use vat photopolymerization 3D printing, which employs light to convert liquid resins into solid objects. Although conventional lightbased 3D printing relies on high energy ultraviolet (UV) light to achieve rapid polymerization rates and correspondingly short build times (approximately seconds per layer), visible light is emerging as an attractive alternative.[11-13] Relative to UV light, visible light is naturally abundant, less expensive, and benign (generally reduced absorption and scattering), which gives it the potential to advance 3D printing of polymeric materials by enabling economical preparation of, for example, cell-laden hydrogels, [14] opaque composites,^[15] or multimaterial structures (via wavelength selective reactions).^[7,16–19]

Recently, we demonstrated that a three component photosystem comprising a visible-light-absorbing photoredox catalyst (PRC) with donor (diphenyliodonium) and acceptor (triphenyl (n-butyl) borate) co-initiators could facilitate photocuring of acrylate-based resins on timescales (approximately seconds) that were competitive with commercial UV light systems (Figure 1).[11] However, the difference in mechanism undergone by UV photoinitiators (PIs) (Type I) and visible PRCs (Type II) to generate reactive radicals results in greater oxygen sensitivity for the latter. Thus, a major limitation of highly reactive visible-light-curable resins for 3D printing is the need for oxygen removal, both from the resin and surrounding atmosphere during printing. To briefly explain the disparity in oxygen sensitivity, UV photoinitiators generate free radicals upon rapid homolytic scission from singlet photoexcited states (Type I mechanism), while efficient visible PRCs often rely on triplet photoexcited states to minimize the impact of ratelimiting electron transfer to a co-initiator for radical formation (Type II mechanism).[20-22] Given that molecular oxygen resides in a triplet ground state, it rapidly reacts with PRCs in their triplet-excited states, which results in a delayed onset of curing, called the oxygen inhibition period.^[23] Furthermore, oxygen will quench propagating carbon centered radicals to form more stable peroxy radicals that do not reinitiate acrylate polymerizations. Thus, oxygen limits curing speed and monomer-topolymer conversion, which necessitates its removal.^[24,25]

www.advmat.de

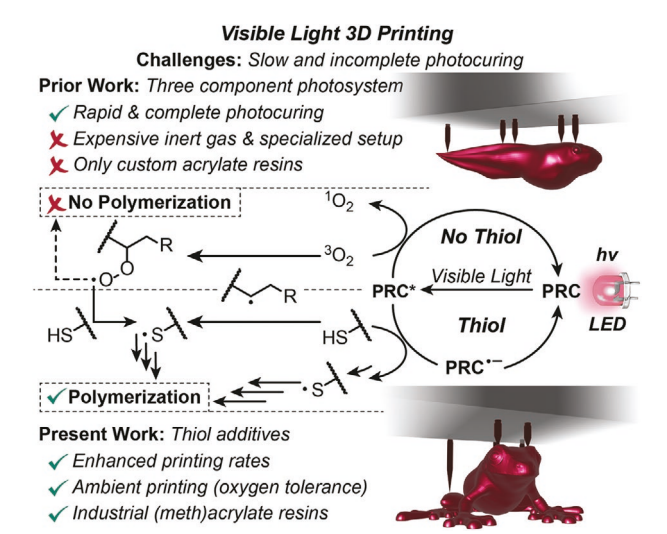


Figure 1. Challenges, prior work, and presented advancements in visible Digital Light Processing (DLP) 3D printing. The central reaction mechanisms show how oxygen inhibits polymerization/curing (top, prior work) and how the addition of thiols bypasses inhibition to generate reactive thiyl radicals that induce polymerization/curing (bottom, present work). The digital 3D renditions of the tadpole and frog relate to prior and present work, respectively, as metaphors for a transformative advance that enables "operation" in air.

Oxygen inhibition time has previously been decreased for photocurable coatings by increasing photocatalyst/photoinitiator concentrations (≥5 wt%), which causes a rapid reaction with ambient oxygen.^[25] However, increased loadings bear a number of limitations, including associated costs, requirements for resin solubility, reduced penetration depths due to optical attenuation, increased toxicity, and plasticization (softening) of cured parts. Alternatively, several physical strategies for eliminating oxygen inhibition have been developed for industrial coatings, such as photocuring under inert gas (e.g., N₂ or Ar), introducing physical barriers (e.g., in-laminate), employing resins with low oxygen solubility, and increasing irradiation intensity.^[25] Despite success in coatings, these approaches limit the general applicability of visible-light 3D printing by requiring specialized and costly equipment. Chemical deoxygenation (e.g., oxygen scavengers) presents a low-cost and facile substitute. Apart from decreasing or removing the oxygen inhibition period, ideal chemical additives should not slow the photopolymerization, generate toxic byproducts that can leach out of the final print, nor alter thermomechanical properties of the printed object.

Inspired by oxygen insensitive thiol—ene photopolymerizations, [26,27] such as that employed by Adaptive 3D Technologies, we examined the use of thiols as additives to enable ambient 3D printing of acrylic resins with red light (≈620 nm). In contrast to pure thiol—ene resins, acrylic resins have a greater commercial presence due to their more tenable odor, improved storage stability, and wider materials scope. Described herein is the unprecedented impact of thiol additives to simultaneously preclude oxygen inhibition and enhance photopolymerization rates under ambient conditions for visible-light photocuring. The process is universal, enabling rapid high-resolution visible-light 3D printing for an array of acrylic resins. To emphasize

industrial relevance, commercial urethane acrylate resins from Dymax serve as a representative case study, where objects with $<\!100~\mu m$ feature dimensions and elastic moduli spanning more than three orders of magnitude are demonstrated. Furthermore, good storage stability and network uniformity without thiol leaching makes the present method an appealing, simple approach to save both time and money in next-generation 3D printing.

2. Results and Discussion

Rapid visible-light 3D printing under ambient conditions required removal of oxygen to minimize inhibition periods. Initially, photocurable resins that undergo a thiol-ene mechanism were considered given the precedent for oxygen insensitivity enabled by rapid and efficient hydrogen atom abstraction from thiols to generate reactive thivl radicals.^[28] For commercial relevance, it was desirable to use industrial (meth)acrylate monomers and crosslinkers as bulk resin constituents. The exemplary resin described below contains an oligourethane diacrylate from Dymax (BR-741) together with tri(propylene glycol) diacrylate (TPGDA) in a 1:1 ratio, pentaerythritol tetrakis(3mercaptopropionate) (PETMP) (1–10 wt%, displacing TPGDA), a three component photosystem, 2,2,6,6-tetramethyl-1-piperidinyloxy (TEMPO), and an opaquing agent (OA) (Figure 2a; Figures S1-S7, Supporting Information). The versatility of this protocol was demonstrated using a wide range of monomers and crosslinkers supplementing those described above: Dymax oligourethane-di(meth)acrylates (BR-345 and BR-952), N,N-dimethylacrylamide, trimethylolpropane triacrylate, isobornyl acrylate, and 2-hydroxyethyl (meth)acrylate (described later and in detail in Table S1 in the Supporting Information). Additionally, nine other small molecules were tested as possible oxygen scavengers, including various thiols, 1.3-diphenylisobenzofuran, triphenylphosphine, and ascorbic acid, all of which underperformed relative to PETMP using equimolar amounts by functionality (details provided in Figures S8 and S9 and Table S9 in the Supporting Information). For clarity, representative experiments are highlighted in the main text, which emphasize resins containing BR-741 and TPGDA.

The combination of BR-741 and TPGDA provides a robust stiff plastic. The tetrathiol, PETMP, was selected to maintain a high crosslink density and corresponding stiffness of the parent acrylate (Figure 2). The three component photosystem comprised zinc tetraphenylporphyrin (ZnTPP) as the red-PRC, 2-(butyryloxy)-N,N,N-trimethylethanlight-absorbing 1-aminium butyltriphenylborate as the electron donor (D) (co-) initiator, and [4-(octyloxy)phenyl](phenyl)iodonium hexafluoroantimonate as the electron acceptor (A) (co-)initiator. This photosystem efficiently generates radicals that can (in the absence of oxygen) result in rapid curing (<10 s) of acrylate-based resins upon exposure to red light (≈620 nm).^[11] A red-light system was chosen, as opposed to green or blue, to emphasize the magnitude of the present results given that rapid photocuring with longer wavelengths of light is inherently more challenging due to the utility of lower energy photons. Inclusion of small amounts of TEMPO (0.01 wt%) as a radical scavenger was found to effectively stabilize the resins and prevent unwanted

www.advmat.de

Figure 2. Primary resin components and proposed mechanisms that enable polymerization under ambient conditions. a) Chemical structures for polymerizable groups. Red-light reactive photosystem: ZnTPP (photoredox catalyst, PRC), borate derivative as electron donor (D) (co-)initiator, and diphenyliodonium derivative as electron acceptor (A) (co-)initiator. Violet-light-reactive photoinitiator (PI), BAPO. b) Mechanism of: i) radical addition to an acrylate to generate a carbon centered radical that ii) reacts with oxygen to form a peroxy radical. iii) The peroxy radical does not react with (meth) acrylate, but iv) abstracts a hydrogen from a thiol to generate a thiyl radical that v) adds to (meth)acrylate via thiol—ene. vi) Radical propagation results in polymer network formation. c) Cycle 1 mechanism: vii) reductive quenching of photoexcited PRC (ZnTPP*) by thiols to generate ZnTPP*— (radical anion) that viii) can be oxidized back to ZnTPP by the diphenyliodonium acceptor, A, and ix) a thiol radical cation that forms a thiyl radical upon H-atom abstraction. x) Thiol—ene addition, followed by xi) H-atom abstraction. Cycle 2 mechanism: xii) energy transfer from ZnTPP* to molecular oxygen (³O₂) forming reactive singlet oxygen (¹O₂) that xiii) can oxidize sulfide to sulfoxide.

background (or "dark") curing (Figures S2 and S3 and Table S4, Supporting Information). The OA selected was Sudan Black, a biological azo-stain^[29] that can passively absorb red light to induce *cis/trans* isomerization and limit the penetration depth of photons to cure only within the layer of interest, similar to the utility of Sudan I in UV/violet active resins.^[30–33] Thus, the presence of OA optimizes 3D printing resolution, particularly in the *z*-dimension (layer thickness), by preventing curethrough. As a control, bis-acylphosphine oxide (BAPO) was employed as a Type I PI operable under 405 nm (violet) light exposure, which replaced the three-component photosystem (Figure 2a).

The addition of PETMP was anticipated to reduce oxygen inhibition through two mechanisms: 1) hydrogen abstraction from thiols by peroxy radicals formed when propagating carbon centered radicals react with molecular oxygen^[34] (Figure 2b) and 2) reductive quenching of ZnTPP* (excited ZnTPP) by thiols^[35] (Figure 2c). While the first mechanism (peroxy radical quenching) has been the predominant rationalization for oxygen tolerance of thiol-ene reactions activated through a Type I UV/violet mechanism, we hypothesize that the second mechanism (reductive quenching) plays a more vital role in the present Type II visible-light photosystem. This is attributed to longlived oxygen reactive PRC triplet states, which facilitate rapid curing with visible light.^[22] Thus, it is proposed that reductive quenching of ZnTPP* (Figure 2c, cycle 1) competes with energy transfer to molecular oxygen (3O2) (Figure 2c, cycle 2), which forms reactive singlet oxygen (¹O₂). Upon reductive quenching, thiol oxidation followed by hydrogen atom transfer^[36] results in the formation of thiyl radicals, which rapidly react with prevalent (meth)acrylate functionality through an anti-Markovnikov thiol–ene addition mechanism. Furthermore, the resultant sulfides (thioethers) may react with $^{1}O_{2}$ to form sulfoxides, $^{[35]}$ precluding deleterious pathways (e.g., $^{1}O_{2}$ reacting with the PRC) that could hamper curing. In this manner, the benefit of thiols for visible-light photocuring (via a Type II mechanism) was proposed to have an unprecedented impact on minimizing the oxygen inhibition period and concomitant build times for emergent 3D printing applications.

To determine the impact of thiol additives on the rate of ambient visible-light photopolymerization, real time Fourier transform infrared spectroscopy (RT FTIR) was used to quantitatively determine monomer-to-polymer conversion during irradiation. Specifically, the disappearance of the signal corresponding to carbon-carbon double bond (C=C) stretches at ≈3100 cm⁻¹ was monitored using a transmission configuration with the resin sample residing in a \approx 100 μ m gap between glass slides (additional experimental details can be found in the "Effect of radical inhibitor on photopolymerization rate and induction period" section in the Supporting Information, including a comparative description of thiol monitoring).[37] All samples showed an excellent temporal response, with no identifiable reactions occurring in the absence of light during the first 10 s of each measurement. Initially, samples without PETMP (tetrathiol) were irradiated under ambient conditions with a red LED centered at 617 nm (full width at half maximum (FWHM) \approx 19 nm) having an intensity of 2.5 mW cm⁻² (matching the DLP 3D printer intensity). For context, commercial UV/violet-light DLP 3D printers that operate at 385-405 nm have reported intensities exceeding 10 mW cm⁻², [38-43] which is

www.advmat.de

significantly higher than the present system and represents a future avenue to examine for improved printing speed and resolution. Red LED illumination resulted in an inhibition period of 49.4 \pm 0.4 s and an initial rate of polymerization of 7.5 \pm 5.3% s^{-1} (immediately following inhibition) (Figure 3a and Table 1). Degassing the same resin (no PETMP) with argon for ≈1 min resulted in a significant decrease in the inhibition period, down to ≈13 s, analogous to prior observations.^[11] However, due to the high viscosity of the Dymax BR-741 containing resin, removal of oxygen by sparging with an inert gas was more challenging than our previous system, [11] resulting in less reproducible inhibition periods. Furthermore, the presence of TEMPO supplements the inhibition period, particularly in the absence of an oxygen scavenger such as thiol (Figures S6 and S7, Supporting Information). The addition of only 1 wt% PETMP reduced the inhibition period to a greater extent than what was typically observed for degassed samples, down to 5.8 ± 1.7 s, while also increasing the polymerization rate up to 19.6 \pm 3.5% s⁻¹.

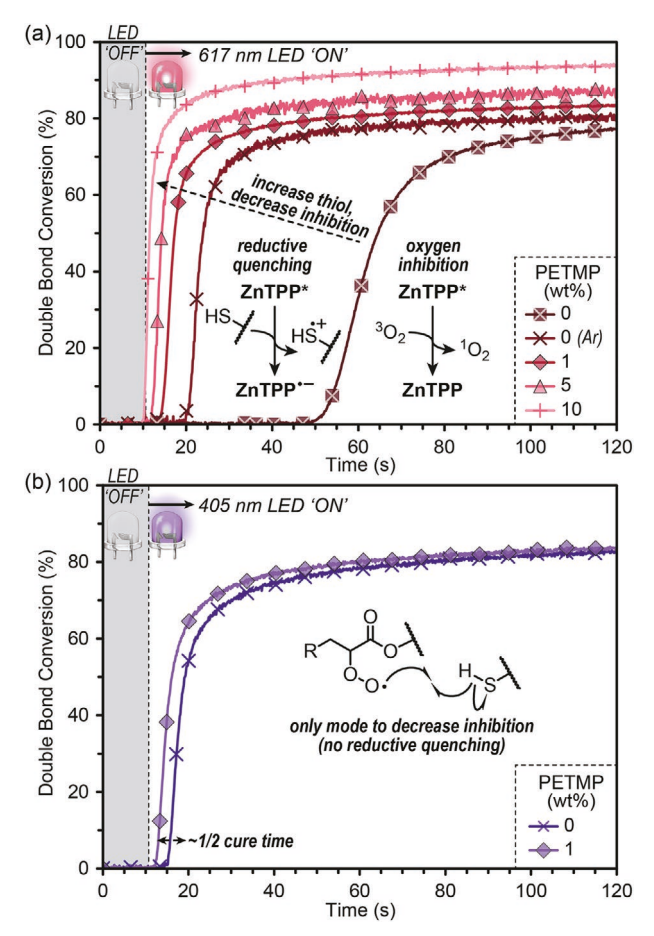


Figure 3. Influence of PETMP (tetrathiol) on oxygen inhibition and rate of BR-741:TPGDA (1:1) polymerization (where PETMP displaces TPGDA), monitored using real-time Fourier transform infrared (RT FTIR) spectroscopy. a) Red-light photocuring (617 nm, 2.5 mW cm⁻²) of resins without PETMP under an ambient (oxygen-containing) and inert (argon) atmosphere, and with 1, 5, and 10 wt% PETMP. b) Violet-light photocuring (405 nm, 3.3 mW cm⁻²) using BAPO as the photoinitiator. A decrease in oxygen inhibition occurs with both red- and violet-light curing, but is more substantial for red light given the combination of reductive quenching and hydrogen atom abstraction by peroxy radicals.

Table 1. Results from RT FTIR measurements shown in Figure 3, highlighting the impact of PETMP (tetrathiol) additives on both the oxygen inhibition period and apparent polymerization rate (R_n) .

-			
PETMP [wt%]	Irradiation wave- length [nm] ^{a)}	Inhibition period [s]	$R_{\rm p} [\% {\rm s}^{-1}]^{\rm b)}$
0	617	49.4 ± 0.4	7.5 ± 5.3
0 (Ar) ^{c)}	617	12.9 ± 3.2	15.9 ± 3.2
1	617	5.8 ± 1.7	19.6 ± 3.5
5	617	1.9 ± 0.5	25.4 ± 2.3
10	617	1.0 ± 0.4	34.0 ± 3.7
0	405	5.2 ± 0.1	13.0 ± 1.0
1	405	2.4 ± 0.2	14.1 ± 0.2

a)An intensity of 2.5 mW cm⁻² for the 617 nm (red) LED and 3.3 mW cm⁻² for the 405 nm (violet) LED was used to match the intensity for Digital Light Processing (DLP) 3D printing described later; b)Rate determined using RT FTIR spectroscopy, monitoring the disappearance of the carbon–carbon double bond (C=C) stretch at 3100 cm⁻¹ to determine the percent conversion of C=C per second immediately following initiation (post-inhibition period); c)The resin was purged with argon for ≈1 min and the measurement was performed under an argon stream.

Photorheology at equivalent light intensity under ambient conditions was in-line with these results, showing a time to gelation (gel point) of 7.9 \pm 0.8 s post-irradiation with 1 wt% PETMP in contrast to a gel point of 64.0 ± 0.6 s without PETMP (Figures S12-S16 and Table S12, Supporting Information). Increasing the content of PETMP further decreased the inhibition time (and gel point) and increased the rate of polymerization, with a nearly instantaneous reaction occurring upon exposure to light when 10 wt% PETMP was incorporated; for reference, 10 wt% PETMP in the present resin corresponds to ≈20 mol% PETMP relative to BR-741 (details provided in the "NMR Spectroscopy" section in the Supporting Information). Preliminary shelf life tests were performed by leaving the resins at room temperature in the dark and testing the photopolymerization kinetics with RT FTIR over time. After four weeks, it was observed that the rate of polymerization and inhibition period remained nearly unchanged, indicating good shelf stability (Figure S11 and Table S11, Supporting Information).

In support of the hypothesis that reductive quenching plays a vital role in minimizing oxygen inhibition, the three-component red-light photosystem was compared to the one component (BAPO) UV/violet photoinitiation, holding everything else constant (Figure 3b and Table 1). Irradiating the BAPO-containing resin with violet light (405 nm and 3.3 mW cm $^{-2}$ to match the DLP printing intensity) resulted in an inhibition period of 5.2 \pm 0.1 s and 2.4 \pm 0.2 s for samples containing 0 and 1 wt% PETMP, respectively. Thus, thiol additives provide a general "drop-in" method to significantly decrease cure time of commercial Type I UV/violet-light-activated resins, and show an even greater impact on Type II visible-light-activated resins. Overall, inhibition can be essentially removed for red-light activated resins via addition of 10 wt% PETMP, and with only 1 wt% PETMP, the resins still cure in under 10 s.

A critical parameter for additively manufactured objects is their mechanical performance, as this often dictates the application space. In particular, polysulfide thermosets from thiolene-based resins often suffer from low stiffness and strength relative to (meth)acrylate-based resins owing to the flexibility of the C–S–C bonds and limited multifunctional thiol starting materials. [44,45] As such, it was deemed important to characterize the impact of PETMP incorporation on mechanical properties, namely, yield strength (σ_y) , stiffness (E, Young's modulus), and strain at fracture (ε_f) . Mechanical dogbone samples (1.11 mm (thickness), 1.76 mm (gauge width), and 18.5 mm (gauge length)) were 3D printed with BR-741:TPGDA (1:1) resins containing 0, 1, 5, and 10 wt% PETMP (where PETMP displaces TPGDA), using red light (\approx 620 nm, 2.5 mW cm⁻²) at an exposure time of 16, 14, 12, and 8 s per layer for resin containing 0, 1, 5, and 10 wt% PETMP, respectively, followed by uniaxial tensile testing (**Figure 4**a). Incorporating 1 wt% PETMP into the resin resulted in samples with nearly identical (slightly

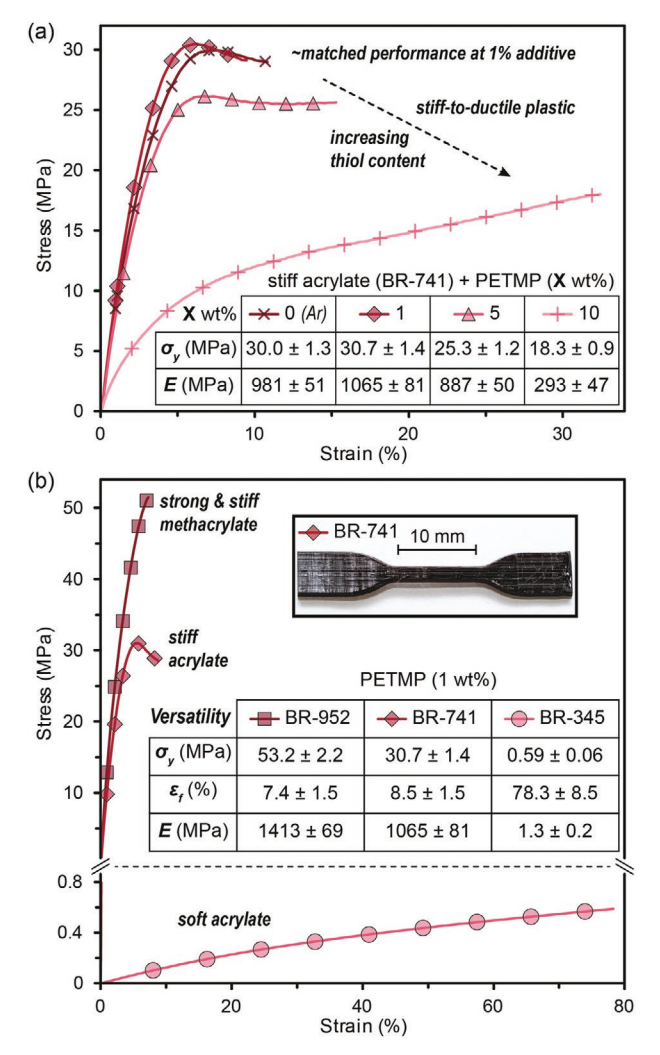


Figure 4. Stress–strain plots of red-light 3D-printed dogbones (1.11 mm (thickness), 1.76 mm (gauge width), and 18.5 mm (gauge length)) under uniaxial tension. a) Influence of PETMP (tetrathiol) content on yield strength (σ_y) and stiffness (E, Young's modulus), showing that the high strength and rigidity can be maintained at low PETMP loading and that samples become more ductile at higher PETMP content. b) Mechanical versatility from ambient visible-light 3D printing with thiol additives, from three industrially relevant Dymax-containing resins. Insets show a representative digital image of the BR-741 dogbone and metrics for σ_y , E, and strain at fracture (E).

improved) performance relative to those printed with no PETMP (under argon)— $\sigma_v \approx 30$ MPa and $E \approx 1000$ MPa. Note, all freshly 3D-printed (green) samples were post-cured with UV light for ≈20 min to reach maximum conversion of vinyl functionality, as is standard practice. As the content of PETMP increased to 5 and 10 wt%, a drop in σ_v and E was observed—25 and 900 MPa (5 wt%) and 18 and 300 MPa (10 wt%), respectively—which may arise from a decrease in crosslink density and/or increase in chain flexibility. Printing the samples with 1 wt% PETMP at three different edge-on angles, horizontal (0°), diagonal (45°), and vertical (90°), provided very similar (approximately isotropic) mechanical performance indicating good adhesion between the layers (Figure S28 and Table S17, Supporting Information). Thus, tailorable mechanical properties with multifunctional thiols was demonstrated, showing a strong and stiff plastic that matches the parent commercial acrylic resin at low thiol contents to a soft and ductile material with higher contents of PETMP, all while enabling rapid, lowenergy visible-light 3D printing under ambient conditions.

To demonstrate the versatility of this platform, two other Dymax resins capable of providing a stronger and more rigid (BR-952) or softer and more compliant (BR-345) material relative to BR-741 were examined (Figure 4b). Specifically, BR-952, a dimethacrylate, was mixed with hydroxyethyl methacrylate (HEMA) and PETMP in a 70/29/1 wt% ratio, while BR-345, a diacrylate, was mixed with hydroxyethyl acrylate and PETMP in a 50/49/1 wt% ratio. In both cases, reproducibly rapid ambient photopolymerization with red light was demonstrated, revealing inhibition periods of 1.2 \pm 0.2 s and $1.3 \pm 0.2 \text{ s}$ and R_p of $6.0 \pm 0.3\% \text{ s}^{-1}$ and $24.5 \pm 0.9\% \text{ s}^{-1}$ for BR-952 and BR-345, respectively (Figure S10 and Table S10, Supporting Information). Notably, this established for the first time that methacrylate-based resins could be 3D printed with visible light, albeit slower than analogous acrylate-based ones. Tensile testing of dogbones prepared from each resin provided distinct mechanical performance, from very strong and stiff $(\sigma_v \approx 53 \text{ MPa} \text{ and } E \approx 1,400 \text{ MPa})$ BR-952, to soft and extensible ($E \approx 1.3$ MPa and $\varepsilon_{\rm f} \approx 80\%$) BR-345. As an added bonus, covalent incorporation of the thiols into the polymer network prevents unpleasant odors and leaching of potentially toxic components-confirmed with gravimetric tests post-solventextraction (Figure S29 and Table S18, Supporting Information) and dynamic mechanical analysis (Figure S30 and Table S19, Supporting Information). These results indicate that addition of multifunctional thiols into commercially relevant acrylic resins represents a universal strategy to increase the rate of photocuring without compromising mechanical performance.

Another important metric in additive manufacturing is feature resolution. To compete with commercial UV/violet-based DLP printing, our proposed system should be capable of providing features with $\leq 100~\mu m$ lateral (x,y) and 25–100 μm vertical (z) resolution. To determine how thiol additives influence the minimum attainable feature size, we used a custom digital method that gave control over exposure time within different locations of a single layer (details provided in the "Optical Profilometry" section in the Supporting Information). The method contained 12 different exposure times per layer, and within each time point, a set of square pillars were present, with varying lateral dimensions from 1 to 16 volume



www.advancedsciencenews.com

ADVANCED MATERIALS

www.advmat.de

elements (voxels) wide. The printer used in this study has a minimum voxel size of $20 \times 20 \mu m^2$ in the lateral dimension and 25 µm in the vertical dimension (i.e., layer thickness). The resolution as a function of PETMP content, number of layers (from 1 to 16), and exposure time per layer (from 2 to 24 s/25 µm layer at 2 s increments) was characterized using optical profilometry for BR-741:TPGDA resins cured with red light (2.5 mW cm⁻²) (full digital images and additional optical profilometry images/analyses are provided Figures S31-S44 in the Supporting Information). The 3D topographical images of representative 12 s per layer time points are shown in Figure 5a and reveal the smallest visible square features as ≈160 µm wide (8 voxels) for no PETMP (argon degassed), ≈80 µm wide (4 voxels) for 1 wt% PETMP, and ≈20 µm wide (single voxel) for 5 and 10 wt% PETMP. Impressively, surface area analysis of the 40 μ m wide squares (2 × 2 voxels) for the 5 wt% PETMP samples revealed an excellent match with the digital input file, while the surface area of 20 µm wide squares was below theoretical values, indicating incomplete curing (Figure S39, Supporting Information). Notably, the square features in the 1 and 5 wt% PETMP prints appear more well defined than those in the 10 wt% prints, which is attributed to a combination of the viscous resin getting trapped in the narrow 20 µm wide cavities separating the squares and cure-through, particularly in the more reactive 10 wt% samples. This was corroborated by measuring the thickness and sidewall angle (SWA) at the corner of each time point to assess z-resolution (Figures S35-S38, Supporting Information). For all samples, the thickness and SWA values nearly matched the digital file, measuring heights of ≈350–400 µm (16 layers at ≈25 µm per layer) and SWAs from \approx 75°-85° (theoretical = 90°). Additionally, the maximum height was reached by 4 and 2 s per layer when incorporating 1 wt%

PETMP and 10 wt% PETMP, respectively, and maintained until the longest time point generated at 24 s per layer. The stability in *z*-height over a wide range of exposure times per layer gave a large operating time window that enhanced reproducibility. This window is attributed to the combined absorption by the PRC (ZnTPP, 0.03 wt%) and OA (0.002 wt% Sudan black) (Figures S45–S47, Supporting Information). However, preliminary analysis suggests that more OA is required to prevent curethrough when printing structures with substantial overhangs (Figure S43, Supporting Information). Altogether, resolution analysis of unoptimized 3D prints using the present ambient visible-light method revealed that small features (<100 μ m) with high x,y,z fidelity (matching the digital input) were easily and reproducibly attainable, rivaling modern UV/violet-based DLP 3D printing technology. [1–3]

To underscore the capabilities of ambient visible-light additive manufacturing, a complex hierarchical object was printed, specifically a 120-cell polytope (or dodecaplex), which is challenging or impossible to produce using traditional manufacturing processes (Figure 5b). The optimized red-light conditions using 1 wt% PETMP with BR-741:TPGDA-based resin were 14 s/25 μ m, which correlates to a build rate of \approx 6.4 mm h⁻¹. Impressively, the object contains 120 dodecahedral cells with the smallest feature size of ≈200 µm. Scanning electron microscopy (SEM) images show the individual ≈25 µm layers from the additive process and emphasize the high feature fidelity. Images of additional complex 3D-printed objects can be found in Figures S46-S48 in the Supporting Information. Uniquely, under UV excitation (365 nm), the objects emit red light, indicating that ZnTPP remains intact during the ambient printing. which provides an avenue toward high-resolution 3D printing of "smart", functional plastics.

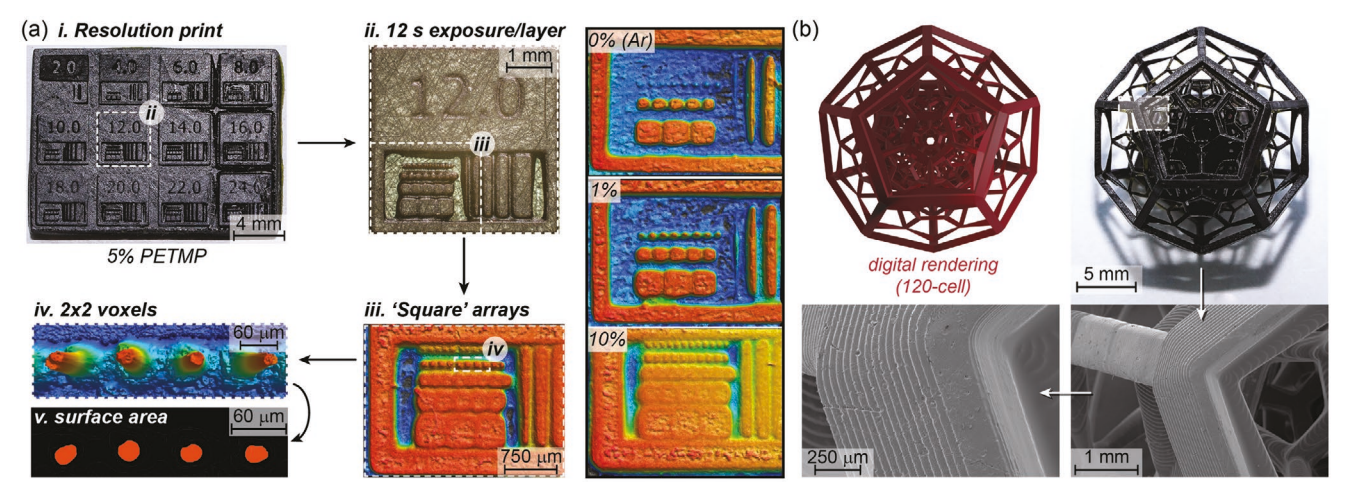


Figure 5. Resolution prints and 3D-printed complex object using red-light DLP with BR-741:TPGDA-based resins (layer thickness = $25 \mu m$). a) Image of a representative resolution print with 5 wt% PETMP (left sequence) and analogous optical profilometry images for 0, 1, and 10 wt% PETMP prints (right). Starting from the top left for the representative sequence is: i) a digital photograph of the full print next to a quarter for reference, showing 12 different exposure times per layer, as indicated by the engraved numbers (representing seconds); ii) optical microscopy image of the 12 s per layer section on the resolution print, which contains arrays of square pillars and lines; iii) 3D topographic image showing square pillars with lateral dimensions varying from 1 to 16 voxels wide (each voxel = $20 \times 20 \times 25 \mu m^3$); iv) optical profilometry of 2 voxels wide square pillars (lateral dimension) and corresponding image analysis showing good fidelity between digital input (1600 μm^2) and printed output (2100 \pm 240 μm^2). Overall, increasing PETMP content results in faster photocuring that provides access to smaller features, but at longer exposures can result in cure-through (loss in z-resolution). b) Representative hierarchical 3D-printed 120-cell using 1 wt% PETMP with the digital rendering (top left), photograph (top right), and SEM images (bottom).



www.advancedsciencenews.com



www.advmat.de

3. Conclusion

Energy efficient visible-light 3D printing under mild ambient conditions was described. A tetrathiol additive (PETMP) as low as 1 wt% in commercially relevant acrylic resins was shown to enable rapid high-resolution 3D printing with low-intensity red light (2.5 mW cm⁻²) in the presence of atmospheric oxygen. Monomer to polymer conversion was monitored using RT FTIR spectroscopy, revealing an excellent temporal response to light exposure in the presence of PETMP, with gelation in less than 3 s, which is comparable to UV/violet-light curing at similar intensities. The dramatic reduction in oxygen inhibition time from ≈49 to ≈6 s in adding 1 wt% PETMP, to essentially complete removal of oxygen sensitivity with 10 wt% PETMP, was attributed to a dual reaction of thiols to form thiyl radicals via hydrogen atom transfer to peroxy radicals and photooxidation by ZnTPP*. Furthermore, direct incorporation of PETMP into the acrylic network via a thiol-ene mechanism mitigates unfavorable odors and leaching of potentially toxic additives. The described method appears to be universal as it works with a range of acrylates, acrylamides, and methacrylates. This provides access to a diverse array of 3D objects with distinct chemical makeup and mechanical properties, from strong and stiff plastics ($\sigma_v \approx 53$ MPa and $E \approx 1400$ MPa) to soft and extensible elastomers ($E \approx 1.3$ MPa and $\varepsilon_f \approx 80\%$). Additionally, the inclusion of PETMP facilitated the formation of fine features with lateral dimensions <50 µm and a layer thickness of 25 μm , all while maintaining a wide processing window (\approx 6–24 s per layer). Finally, 3D printing of a hierarchical 120-cell polytope highlighted the capabilities offered by the present technique to harness custom objects with digitally defined form factors. This simple approach presents numerous opportunities to create next-generation advanced materials in a mild additive fashion using visible-to-near infrared light, which will positively impact many arenas beyond 3D printing, from coatings and adhesives to imaging. Within 3D printing, it is envisioned that longer wavelengths of light will facilitate the fabrication of functional materials that are otherwise sensitive to UV/violet light (e.g., biomaterials and composites) used in contemporary DLP technology, while also enabling the construction of multifunctional materials using different wavelengths of light to activate distinct chemical reactions. Moreover, a number of fundamental scientific questions are now available to be addressed, such as how various metrics (e.g., light dosage and wavelength) and resin compositions influence the speed, resolution, and material properties of visiblelight-reactive resins. Currently, we are leveraging this new knowledge for 3D printing of hydrogels and multimaterial structures with applications in tissue engineering and soft robotics.

Supporting Information

Supporting Information is available from the Wiley Online Library or from the author.

Acknowledgements

D.A. and L.M.S. contributed equally to this work. The authors thank the Robert A. Welch Foundation (F-2007) and the Center for Dynamics and Control of Materials: An NSF MRSEC (DMR-1720595) for financial

support. The authors acknowledge the use of shared research facilities supported in part by the Texas Materials Institute, the Center for Dynamics and Control of Materials: An NSF MRSEC (DMR-1720595), and the NSF National Nanotechnology Coordinated Infrastructure (ECCS-1542159). The authors thank Dr. Yun-Ho Jang at MonoPrinter for help with the custom DLP 3D printer and Dymax for supplying a range of urethane (meth) acrylate oligomers for this study.

Conflict of Interest

The authors declare no conflict of interest.

Data Availability Statement

The data that support the findings of this study are available from the corresponding author upon reasonable request.

Keywords

3D printing, Digital Light Processing, photochemistry, photocuring, polymers

Received: June 26, 2021 Published online: September 14, 2021

- [1] R. L. Truby, J. A. Lewis, Nature 2016, 540, 371.
- [2] A. Bagheri, J. Jin, ACS Appl. Polym. Mater. 2019, 1, 593
- [3] T. J. Wallin, J. Pikul, R. F. Shepherd, Nat. Rev. Mater. 2018, 3, 84
- [4] J. R. Tumbleston, D. Shirvanyants, N. Ermoshkin, R. Janusziewicz, A. R. Johnson, D. Kelly, K. Chen, R. Pinschmidt, J. P. Rolland, A. Ermoshkin, E. T. Samulski, J. M. DeSimone, *Science* 2015, 347, 1349.
- [5] M. P. De Beer, H. L. Van Der Laan, M. A. Cole, R. J. Whelan, M. A. Burns, T. F. Scott, Sci. Adv. 2019, 5, eaau8723.
- [6] D. G. Moore, L. Barbera, K. Masania, A. R. Studart, *Nat. Mater.* 2019, 19, 212
- [7] J. J. Schwartz, A. J. Boydston, Nat. Commun. 2019, 10, 791.
- [8] D. A. Walker, J. L. Hedrick, C. A. Mirkin, Science 2019, 366, 360.
- [9] S. K. Saha, D. Wang, V. H. Nguyen, Y. Chang, J. S. Oakdale, S. C. Chen, *Science* 2019, 366, 105.
- [10] A. Vyatskikh, S. Delalande, A. Kudo, X. Zhang, C. M. Portela, J. R. Greer, Nat. Commun. 2018, 9, 593.
- [11] D. Ahn, L. M. Stevens, K. Zhou, Z. A. Page, ACS Cent. Sci. 2020, 6, 1555.
- [12] A. Bagheri, C. W. A. Bainbridge, K. E. Engel, G. G. Qiao, J. Xu, C. Boyer, J. Jin, ACS Appl. Polym. Mater. 2020, 2, 782.
- [13] L. Zhang, X. Shi, Z. Zhang, R. P. Kuchel, R. Namivandi-Zangeneh, N. Corrigan, K. Jung, K. Liang, C. Boyer, Angew. Chem., Int. Ed. 2021, 60, 5489.
- [14] K. S. Lim, J. H. Galarraga, X. Cui, G. C. J. Lindberg, J. A. Burdick, T. B. F. Woodfield, Chem. Rev. 2020, 120, 10662.
- [15] B. Strehmel, C. Schmitz, K. Cremanns, J. Göttert, Chem. Eur. J. 2019, 25, 12855.
- [16] N. D. Dolinski, Z. A. Page, E. B. Callaway, F. Eisenreich, R. V. Garcia, R. Chavez, D. P. Bothman, S. Hecht, F. W. Zok, C. J. Hawker, Adv. Mater. 2018, 30, 1800364.
- [17] S. Bialas, L. Michalek, D. E. Marschner, T. Krappitz, M. Wegener, J. Blinco, E. Blasco, H. Frisch, C. Barner-Kowollik, Adv. Mater. 2019, 31, 1807288.



www.advancedsciencenews.com

ADVANCED MATERIALS

www.advmat.de

- [18] V. Hahn, P. Kiefer, T. Frenzel, J. Qu, E. Blasco, C. Barner-Kowollik, M. Wegener, Adv. Funct. Mater. 2020, 30, 1907795.
- [19] L. Michalek, S. Bialas, S. L. Walden, F. R. Bloesser, H. Frisch, C. Barner-Kowollik, Adv. Funct. Mater. 2020, 30, 2005328.
- [20] N. S. Allen, J. Photochem. Photobiol., A 1996, 100, 101.
- [21] P. Lu, K.-Y. Chung, A. Stafford, M. Kiker, K. Kafle, Z. A. Page, *Polym. Chem.* 2021, 12, 327.
- [22] A. Stafford, D. Ahn, E. K. Raulerson, K. Y. Chung, K. Sun, D. M. Cadena, E. M. Forrister, S. R. Yost, S. T. Roberts, Z. A. Page, J. Am. Chem. Soc. 2020, 142, 14733.
- [23] D. M. Arias-Rotondo, J. K. McCusker, Chem. Soc. Rev. 2016, 45, 5803.
- [24] N. Rostami, D. Graf, L. Schranzhofer, S. Hild, T. Hanemann, Prog. Org. Coatings 2019, 130, 221.
- [25] S. C. Ligon, B. Husár, H. Wutzel, R. Holman, R. Liska, Chem. Rev. 2014, 114, 557.
- [26] L. Chen, Q. Wu, G. Wei, R. Liu, Z. Li, J. Mater. Chem. C 2018, 6, 11561.
- [27] C. C. Cook, E. J. Fong, J. J. Schwartz, D. H. Porcincula, A. C. Kaczmarek, J. S. Oakdale, B. D. Moran, K. M. Champley, C. M. Rackson, A. Muralidharan, R. R. McLeod, M. Shusteff, Adv. Mater. 2020, 32, 2003376.
- [28] F. Dénès, M. Pichowicz, G. Povie, P. Renaud, Chem. Rev. 2014, 114, 2587.
- [29] D. P. Penney, J. M. Powers, M. Frank, C. Willis, C. Churukian, Biotech. Histochem. 2002, 77, 237.
- [30] A. Reid, J. C. Jackson, J. F. C. Windmill, Soft Matter 2020, 17, 1881.
- [31] N. A. Traugutt, D. Mistry, C. Luo, K. Yu, Q. Ge, C. M. Yakacki, Adv. Mater. 2020, 32, 2000797.

- [32] D. G. Moore, L. Barbera, K. Masania, A. R. Studart, *Nat. Mater.* 2020, 19, 212.
- [33] K. Kowsari, B. Zhang, S. Panjwani, Z. Chen, H. Hingorani, S. Akbari, N. X. Fang, Q. Ge, Addit. Manuf. 2018, 24, 627.
- [34] C. E. Hoyle, T. Y. Lee, T. Roper, J. Polym. Sci., Part A: Polym. Chem. 2004, 42, 5301.
- [35] A. Guerrero-Corella, A. María Martinez-Gualda, F. Ahmadi, E. Ming, A. Fraile, J. Alemán, Chem. Commun. 2017, 53, 10463.
- [36] L. Capaldo, D. Ravelli, Eur. J. Org. Chem. 2017, 2017, 2056.
- [37] S. Chatani, T. Gong, B. A. Earle, M. Podgorski, C. N. Bowman, ACS Macro Lett. 2014, 3, 315.
- [38] J. Zhang, F. Dumur, P. Xiao, B. Graff, D. Bardelang, D. Gigmes, J. P. Fouassier, J. Lalevée, *Macromolecules* 2015, 48, 2054.
- [39] M. Caprioli, I. Roppolo, A. Chiappone, L. Larush, C. F. Pirri, S. Magdassi, Nat. Commun. 2021, 12, 2462.
- [40] P. Sautrot-Ba, V. Brezová, J. P. Malval, A. Chiappone, L. Breloy, S. Abbad-Andaloussi, D. L. Versace, *Polym. Chem.* 2021, 12, 2627.
- [41] Y. Shen, H. Tang, X. Huang, R. Hang, X. Zhang, Y. Wang, X. Yao, Carbohydr. Polym. 2020, 235, 115970.
- [42] J. Wang, S. Stanic, A. A. Altun, M. Schwentenwein, K. Dietliker, L. Jin, J. Stampfl, S. Baudis, R. Liska, H. Grützmacher, Chem. Commun. 2018, 54, 920.
- [43] L. Pezzana, G. Riccucci, S. Spriano, D. Battegazzore, M. Sangermano, A. Chiappone, *Nanomaterials* 2021, 11, 373.
- [44] H. B. Song, A. Baranek, B. T. Worrell, W. D. Cook, C. N. Bowman, Adv. Funct. Mater. 2018, 28, 1801095.
- [45] M. Sahin, S. Ayalur-Karunakaran, J. Manhart, M. Wolfahrt, W. Kern, S. Schlögl, Adv. Eng. Mater. 2017, 19, 1600620.